ESTIMATION OF DIFFUSION CHAMBER BIOCOMPATIBILITY IN THE EXPERIMENTAL MODEL OF IMPLANTATION IN THE NEUROVASCULAR BUNDLE

Marzol EA✉, Dvornichenko MV, Mitryaikin NS, Aparshev NA

Siberian State Medical University, Tomsk, Russia

Polycaprolactone as a material used when constructing nanocomposite structures is sufficiently studied in terms of therapeutic effect and safety of use. However, its biocompatibility in the form of three-dimensional carrier macrochambers is still a matter of debate due to changes in the way the 3D printing is done. The study was aimed to determine biocompatibility of the diffusion chamber made of polycaprolactone after implantation in the rat femoral neurovascular bundle. The study involved mature male Wistar rats. Animals of group 1 (experimental, *n* = 4) underwent implantation of the polycaprolactone diffusion chamber in the femoral neurovascular bundle. Group 2 (control, *n* = 3) included intact rats. Macroscopic assessment revealed no abnormalities at the site of implantation and in the target organs. Tissue microscopy revealed no systemic response; the number of binucleated hepatocytes was 1.05%. The stromal–parenchymal relationship values were as follows: liver — 1/33.20, adrenal glands — 1/19.53, kidney — 1/23.65, spleen — 1/26.52. On day 40, hemogram showed the increase in lymphocyte counts by 4%, the decrease in segmented neutrophil counts by 17% and monocyte counts by 17%. These findings confirm safety of using the polycaprolactone diffusion chamber and its biocompatibility when installed in the large neurovascular bundle. However, the effects of polycaprolactone degradation products require more extensive study over the longer periods of biointegration.

Keywords: diffusion chambers, polycaprolactone, biocompatibility, cell technologies, systemic reaction, microfluidic technologies

Funding: the study was supported by the RSF (research project No. 23-25-00346).

Author contribution: Marzol EA, Dvornichenko MV — developing concept and design; Marzol EA, Aparshev NA, Mitryaikin NS — data analysis and interpretation; Marzol EA, Mitryaikin NS, Dvornichenko MV — substantiation of manuscript or verification of critical intellectual content; Dvornichenko MV — final approval of manuscript before publishing.

Compliance with ethical standards: the study was approved by the Ethics Committee of the Siberian State Medical University (protocol No. CDI-005 dated 5 February 2022). Animals were handled in accordance with the Directive 2010/63/EU of the European Parliament and the Council on the protection of animals used for scientific purposes dated 22 September 2010, rules and regulations of the European Community (86/609EEC), Declaration of Helsinki, and orders of the Ministry of Health of the USSR (No. 742 dated 13 November 1984 and No. 48 dated 23 January 1985).

✉ **Correspondence should be addressed:** Ekaterina A. Marzol
Kartashova, 29b, kv. 78, Tomsk, 634 041; Katya4803@mail.ru

Received: 27.06.2024 **Accepted:** 21.07.2024 **Published online:** 19.08.2024

DOI: 10.24075/brsmu.2024.032

ОЦЕНКА БИОСОВМЕСТИМОСТИ ДИФФУЗИОННЫХ КАМЕР В ЭКСПЕРИМЕНТАЛЬНОЙ МОДЕЛИ ИМПЛАНТАЦИИ НА СОСУДИСТО-НЕРВНОМ ПУЧКЕ

Е. А. Марзоль✉, М. В. Дворниченко, Н. С. Митряйкин, Н. А. Апаршев

Сибирский государственный медицинский университет, Томск, Россия

Поликапролактон как материал при создании нанокомпозитных структур достаточно изучен с позиции терапевтического эффекта и безопасности применения. Однако его биосовместимость в виде объемных макрокамер-носителей остается предметом дискуссии ввиду изменения способа 3D-печати. Целью работы было определить биосовместимость диффузионной камеры из поликапролактона при ее имплантации на бедренный сосудисто-нервный пучок крысы. Исследование проводили на половозрелых крысах-самцах линии Wistar. Животным группы 1 (экспериментальная, *n* = 4) проводили имплантацию диффузионной камеры из поликапролактона на бедренный сосудисто-нервный пучок. В группу 2 (контрольная, *n* = 3) вошли интактные крысы. В ходе макроскопической оценки не было выявлено патологических изменений на месте имплантации и в органах-мишенях. При микроскопии тканей не выявлено системной реакции, количество двуядерных гепатоцитов составило 1,05%. Показатели стромально-паренхиматозного отношения составили: печень — 1/33,20, надпочечники — 1/19,53, почки — 1/23,65, селезенка — 1/26,52. На 40-е сутки картина крови включала в себя повышение числа лимфоцитов на 4%, уменьшение сегментоядерных нейтрофилов на 17% и моноцитов на те же 17%. Эти результаты подтверждают безопасность использования диффузионной камеры из поликапролактона и ее биосовместимость при постановке на крупные сосудистно-нервные пучки, однако влияние продуктов биодеградации поликапролактона требует более широкого исследования при более длительных сроках биоинтеграции.

Ключевые слова: диффузионная камера, поликапролактон, биосовместимость, клеточные технологии, системная реакция, микрофлюидные технологии

Финансирование: исследование выполнено при финансовой поддержке РНФ в рамках научного проекта №23-25-00346.

Вклад авторов: Е. А. Марзоль, М. В. Дворниченко — разработка концепции и дизайна; Е. А. Марзоль, Н. А. Апаршев, Н. С. Митряйкин — анализ и интерпретация данных; Е. А. Марзоль, Н. С. Митряйкин, М. В. Дворниченко — обоснование рукописи или проверка критически важного интеллектуального содержания; М. В. Дворниченко — утверждение рукописи.

Соблюдение этических стандартов: исследование одобрено этическим комитетом Сибирского государственного медицинского университета (протокол № ЦДИ-005 от 5 февраля 2022 г.). Все манипуляции с животными проводили в соответствии с директивой Европейского Парламента № 2010/63EU от 22.09.2010 «О защите животных, используемых для научных целей», с соблюдением правил и норм Европейского общества (86/609EEC), Хельсинкской декларации и приказов Министерства здравоохранения СССР (№ 742 от 13.11.1984 и № 48 от 23.01.1985).

✉ **Для корреспонденции:** Екатерина Александровна Марзоль
ул. Карташова, 29б, кв. 78, г. Томск, 634 041; Katya4803@mail.ru

Статья получена: 27.06.2024 **Статья принята к печати:** 21.07.2024 **Опубликована онлайн:** 19.08.2024

DOI: 10.24075/vrgmu.2024.032

Materials showing maximum biocompatibility after implantation, including polycaprolactone, polyvinylpyrrolidone, polyglycolic acid, etc., are currently used in tissue modeling [1–2]. In this row polycaprolactone (PCL), a synthetic polymer belonging to the class of aliphatic polyesters that was synthesized in early 1930s, is the most promising for bioengineered constructs [3]. Its specific physical-chemical and mechanic properties, viscoelasticity, and ease of molding resulted in production of products of various shapes for biomedical sphere: from suturing to replacement of organs and tissues using 3D printing, particularly, 3D printing of isolation (diffusion) chambers for implantation of cellular material. To date, the nanocomposite modifications and additive technologies to fabricate polycaprolactone scaffolds for regenerative medicine have been studied in terms of both therapeutic efficacy and safety of use [4]. However, forming three-dimensional hollow carrier macrochambers for cellular material (diffusion chambers), allowing one to some extent isolate the chamber content from the recipient organism environment and not losing sufficient adhesion properties, from polycaprolactone requires modification of 3D printing conditions, which results in alteration of the material fibers' density and architecture and, therefore, changes its physical-chemical properties and biocompatibility degree [5–6]. It has been proven that PCL shows low bioresorption counter to moderate biodegradation, which can be adjusted by changing the volume of the structure formed, polarization, or additional administration of anti-inflammatory cytokines [7–8]. The PCL degradation parameters depend on molecular weight, polymer shape, and implantation localization, specifically on the degree of vascularization. According to this, both complete elimination of products yielding carbon dioxide, caproic acid, and water and breakdown to intermediate polymer crystals, 6-hydroxycarboxylic acid, amorphous colloids being the components of macrophage endosomes are possible [9]. The studies of such constructs are most often conducted at the level of foreign body reaction (FBR) considering local tissue alterations, immune response morphology *in situ*, and resorptive potential within a short period of time, which makes it possible to partially exponentially estimate the terms of possible implantation, half-life, and possible consequences for the host [1, 10–11]. However, this approach does not allow us to claim with confidence that morphofunctional alterations, including the increase in osmotic pressure relative to the surrounding tissues, pH shift to the acidic side, low-grade productive inflammation and undulating oxidative stress associated with uneven autocatalytic cleavage of the low molecular weight fragments, are just local [12–14].

Under conditions of the diffusion chamber installation in the neurovascular bundle (NVB) the direct transfer of PCL crystals and breakdown products into bloodstream by macrophages is the bioresorption criterion [15–16], which in combination with the material physical-chemical properties can change both qualitative characteristics of the blood vessel and cellular makeup of the capsule, possibly leading to the more acute oxidative stress in the host at both local (at the construct installation site) [17] and systemic [18] levels.

Thus, there is a need to study the effects of polycaprolactone biodegradation products and general significance of implantation at the local and systemic morphofunctional levels, which can be achieved under conditions of using a diffusion chamber in the rat femoral NVB *in vivo* [19].

The study was aimed to determine biocompatibility of the polycaprolactone diffusion chamber, when implanted in the rat femoral neurovascular bundle.

METHODS

A diffusion chamber (DC) was designed using the Blender open-source software and made of polycaprolactone (Natural works Ingeo 40-43d NatureWorks LLC) by Fused Filament Fabrication involving filaments obtained by electrospinning using the CreatBot Duo 3D printer (CreatBot 3D Printer; China). The chamber consisted of two parts connected with the latches to form a hollow capsule with grooves in the end walls (Fig. 1), which made it possible to fix the chamber on the NVB. The chamber material represented a biodegradable polyester (PCL 100%) that was allowed for medical use and had low melting point (59–64 °C).

The DC was sterilized with the 100% ethylene oxide vapor at 37 °C for 9 h in the 3M Steri-Vac Sterilizer/Aerator (3M; USA) in accordance with the guidelines (GOST ISO 11135-2017).

Wistar rats with the body weight of 280–300 g kept under standard vivarium conditions without antibiotic therapy at the laboratory of biological models of the Siberian State Medical University (Tomsk) were used as experimental models. The animals were divided into two groups for the experiment: the experimental group 1 (n = 4) included animals with the DC implanted in the femoral NVB; the control group 2 (n = 3) included intact rats. DCs were implanted to experimental animals under isoflurane anesthesia. Atropine in a dose of 0.2 mg/kg was administered intramuscularly 15 min before surgery in order to prevent intraoperative complications. Surgical approach began from the 2–3 cm incision, deep in the inguinal fold, in the inward direction from the femoral artery pulsation (Fig. 1).

The animals were euthanized through CO_2 inhalation 40 days after the end of the experiment. Macroscopic (visual) assessment of the implantation site was performed on days 3, 7, 12, as well as 40 days after the beginning of the experiment during necropsy; assessment was performed based on blood filling of blood vessels, incapsulation, and visual signs of inflammation (presence of hyperemia, edema, infiltration) in points, where score 0 meant no sign, score 1 meant mild degree, score 2 meant moderate degree.

To assess the recipient's reactive response, we collected the tail vein blood smears before implantation and on day 40 after implantation. Blood smears were Romanovsky–Giemsa stained. Histological specimens of the target organs (liver,

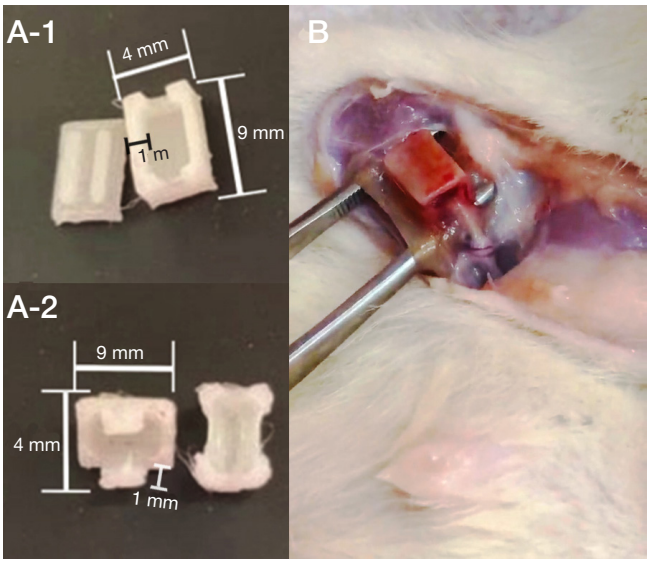

Fig. 1. A–1, A–2. Parameters of the experimental of the PCL DC (length — 9 mm, width — 4 mm, thickness — 1 mm). **B**. Surgical site of the DC (PCL) implantation

Table 1. Macroscopic parameters of polycaprolactone diffusion chambers implanted in the femoral neurovascular bundles of the Wistar rats

Study groups	Inflammation	Hyperemic implantation site	Chamber incapsulation
Experimental group	0	1	1,5
n = 4	(0–0)	(1–1.5)	(1–1.5)
Control group	0	0	–
n = 3	(0–0)	(0–1)	

spleen, kidney, adrenal glands) were prepared after necropsy by the standard method involving hematoxylin and eosin staining [20]. Miscroscopy was performed using the Karl Zeiss Observer D1 light microscope (Carl Zeiss; Germany).

Morphometry aimed to estimate possible reactive changes of the organs was performed based on the images acquired with the Zeiss AxioCam ICc5 digital camera for light microscopy (Carl Zeiss; Germany). It was based on the stromal–parenchymal relationship: stromal components (blood vessels, interstitial tissue, septal areas, capsule)/parenchyma, as well as on determination of the percentage of binucleated hepatocytes per 100 cells. Hematogram was assessed based on the white blood cell differential. A total of 10 fields of view per group were assessed to calculate the parameters. Statistical processing was performed using the Statistica 10.0, IBM software (TIBCO Software; USA). Statistical hypotheses were tested for the trait distribution normality using the Shapiro–Wilk test for small ($n < 30$) samples. Descriptive and nonparametric statistics were used to process the results obtained. The studied parameters were described as the median (Me), 25% (Q_1) and 75% (Q_3) quartiles. The Mann–Whitney *U* test and the median test were used when comparing independent samples; the Friedman test was used for pairwise comparison. The differences were considered significant at $p < 0.05$.

RESULTS

Behavior, appearance, and haircoat of rats in the experimental group were the same as that of control animals throughout the period of experimental modeling of the DC implantation in the NVB. No local postoperative complications were revealed; the operated limb mobility was preserved and remained unchanged.

The studied biocompatibility parameters are provided in Table 1.

The anatomic and topographic state of the studied internal organs (kidney, adrenal glands, spleen, liver) of animals in the experimental group showed no differences from the control group.

Macroscopic assessment of the organs of animals in the experimental group revealed no typical lesions or alterations (normally colored organs with the even surface, intact, not enlarged, showing no signs of atrophy, fibrosis, scarring, the capsule was preserved, not thickened) compared with the organs of control animals.

Microscopic examination of the liver in rats of the control group (Fig. 2) showed the following: the non-thickened Glisson's fibrous capsule, lobules of irregular hexagonal shape were visible at low magnification, the boundaries between the lobules were unclear due to underdeveloped connective tissue, the triad structure was preserved. No lesions or alterations were revealed.

At high magnification, the lobules consisted of the radially arranged hepatic cords representing the anastomosing strands of hepatocytes. The liver sinusoids lined with endothelial cells were located between the cords. The portal tract consisting of the interlobular artery, the vein (the vein was 3–4 times larger in diameter, than the artery), bile duct duct lined with a single layer of cuboidal epithelium with the large, dark, round nuclei and surrounded by the connective tissue envelope, and the interlobular lymphatic vessel was visible in close vicinity to the lobule. Hepatocytes were mostly mononuclear, with the clearly visible basophilic nuclei and homogeneous dark red cytoplasm. The relative binucleated hepatocyte counts per 100 cells in the fields of view were 1.05% (1.02%; 1.11%), i.e. less than 10%.

Interstitial tissue was visible showing no infiltration, proliferation or signs of fibrosis. Blood vessels were represented by the central veins located in the center of the hepatic lobules, sublobular veins having a significantly larger lumen, gathering veins located between the lobules, portal tract (sporadic lymphocytes, monocytes, and histiocytes were found), sinusoids. The lumen was the same in the visible field, the walls were unchanged, there were no cell infiltration or signs of extravasation.

Microscopic examination of the adrenal glands in rats of the experimental group (Fig. 3) showed the following: the non-thickened fibrous capsule, and the boundary between the cortex and medulla were visible at low magnification. The cortex consisted of the zona glomerulosa, zona fasciculata, and zona reticularis. The medulla contained the darker and larger cells. No lesions or alterations were revealed.

At high magnification, the zona glomerulosa was represented by small monomorphic cells with the evenly stained oxyphilic cytoplasm and the eccentrically located nuclei, forming the racemose patterns. Sporadic larger cells with polymorphic nuclei were visible. The zona fasciculata was larger, the cortical plateau consisted of branching divergent sinusoids, between which the cords of oxyphilic, vacuolated, mostly large cells with hyperchromatic nuclei were located. The boundary between the zona fasciculata and zona reticularis was determined by the connective tissue layer. The zona reticularis was represented by small blood vessels, intensely colored round and angulate cells with small hyperchromatic nuclei.

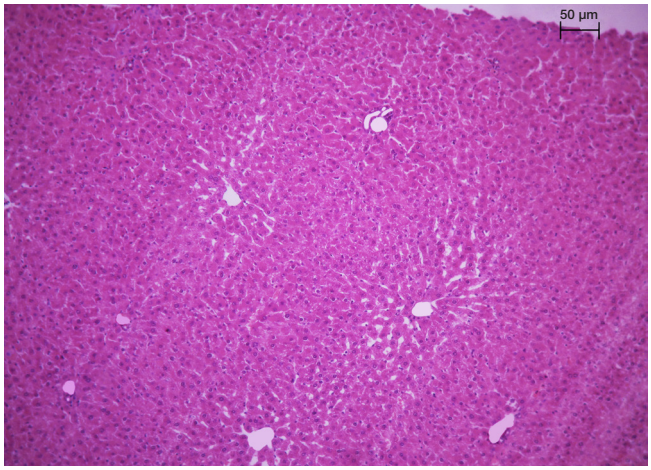

Fig. 2. Microscopic slices of the liver of Wistar rats of the experimental group (with the implanted PCL DC). Hematoxylin and eosin; 10× magnification

The medulla was visible as the vascular network, large parenchymal cells forming dense cords, large light nucleus, vacuolated cytoplasm; punctate granulation was revealed. Wide efferent gathering veins and sinusoid capillaries surrounded by the chromaffin cells with basophilic cytoplasm were determined.

Interstitial tissue was visible showing no infiltration or proliferation. The lumen was the same in the visible field, the walls were unchanged, there were no cell infiltration or signs of extravasation.

Microscopic examination of the spleen in rats of the experimental group (Fig. 4) showed the following: the non-thickened fibrous capsule, from which the ill-defined trabeculae anastomosing with each other radiated, was visible at low magnification. The boundary between the white and red pulp was preserved. The white pulp constituted 1/5 of the organ, it was diffusely distributed, mainly subcapsularly. The red pulp constituted the remaining part of the organ (without the capsule and trabeculae), it consisted of the splenic capillaries and splenic cords. No lesions or alterations were revealed.

At high magnification, the oxiphilic capsule composition was as follows: mesothelium, dense fibrous tissue, and smooth muscle cells. The oxiphilic trabeculae consisted of collagen fibers and smooth muscle cells. There was the splenic pulp with the reticular tissue framework between the trabeculae. The splenic white pulp was represented by the lymphoid tissue of the lymphoid nodules (lymphocyte clusters) and periarteriolar lymphoid sheaths (composition: reticular cells, lymphocytes, macrophages, plasma cells), surrounding the arteries at the exit from the trabeculae. Lymphocytes, macrophages, reticular cells were visible in the lymphoid nodule crowns, while lymphocytes at various stages of proliferation and differentiation, plasma cells, macrophages were visible in the germinal center. The mantle zone (cluster of memory B cells and proplasmocytes) surrounded the periarteriolar and reactive areas. The nodule marginal zone was surrounded by the sinusoid capillaries. The main components of the red pulp were reticular tissue with blood cells (erythrocytes, granular and non-granular leukocytes) and sinusoids anastomosing with each other.

Interstitial tissue was visible showing no infiltration or proliferation. Blood vessels were represented by the trabecular veins, trabecular arteries, pulp arteries (around which T cells accumulated), central arteries located eccentrically on the periphery of the follicle, venous sinuses and capillaries. The lumen was the same in the visible field, the walls were unchanged, there were no cell infiltration or signs of extravasation.

Microscopic examination of the rat kidney in the experimental group also showed that the organ had a typical structure: the non-thickened fibrous capsule was visible at low magnification, the boundary between the renal cortex and medulla was preserved. The renal cortex included the renal corpuscles, the system of convoluted tubules radially converging to the medulla consisting of the straight tubules. No lesions or alterations were revealed.

At high magnification, the renal corpuscle was represented by the glomerule of capillaries, non-thickened external capsule, the parietal and visceral layers of which fitted tightly together; the Bowman's space was almost invisible. The histological slice showed proximal convoluted tubules, the single-layer cubic epithelium of which showed oxiphilic staining, basophilic nuclei. The lumens of these tubules were narrow and free. Distal tubules with the wide lumen were lined with the columnar epithelium having opalescent cytoplasm, no rim was visible, a dense spot was visible in the surroundings. The medulla was represented by the straight tubules and the collecting ducts.

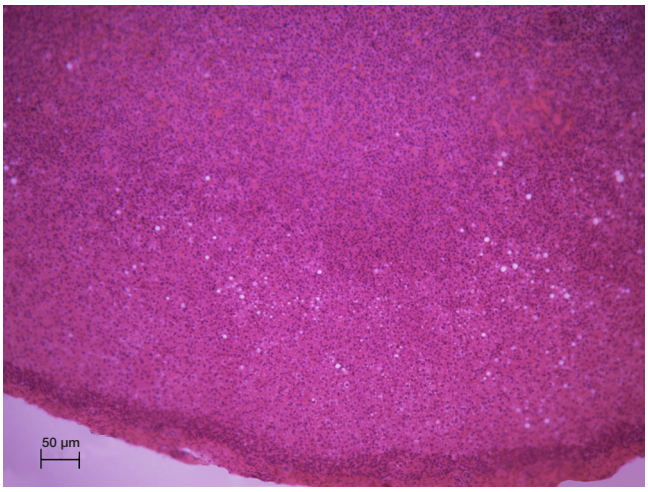

Fig. 3. Microscopic slices of the adrenal glands of Wistar rats of the experimental group (with the implanted PCL DC). Hematoxylin and eosin; 10× magnification

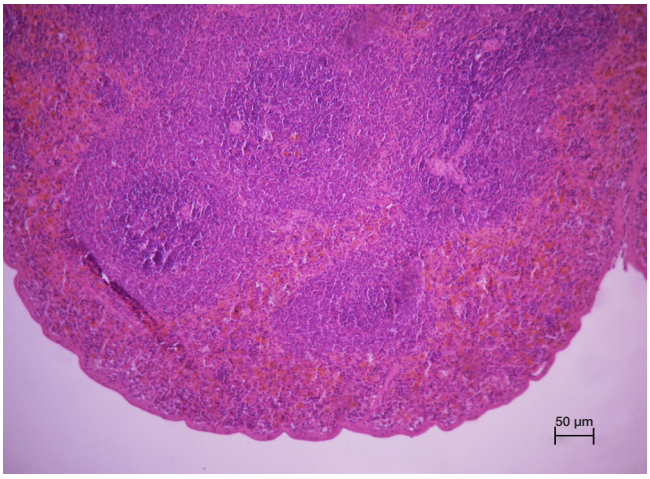

Fig. 4. Microscopic slices of the spleen of Wistar rats of the experimental group (with the implanted PCL DC). Hematoxylin and eosin; 10× magnification

The straight tubules with the narrow lumen were represented by the single-layer cuboidal brush border epithelium. The collecting ducts with the free lumen consisted of the single-layer cuboidal epithelium showing paler oxiphilic staining, the nuclei were located closer to the lumen. No lesions or alterations were revealed.

Interstitial tissue was visible showing no infiltration, it occupied an interstitial position relative to the parenchyma, there was no proliferation. Blood vessels were represented by the subcapsular veins, afferent arteries, interlobular arteries and veins in the cortex and arcuate arteries and veins in the medulla. The lumen was the same in the visible field, the walls were unchanged, there were no cell infiltration or signs of extravasation.

Descriptive assessment of the morphometric parameter, the stromal–parenchymal relationship, in the control group of animals showed no significant differences from the experimental group. The following values of the studied parameter were obtained when assessing the adrenal gland histological specimen: control — 1/21.21 (1/21.27; 1/23.13), experiment — 1/19.53 (1/17.85; 1/20.56); calculation for the microscopic slices of rat liver showed that the value of the parameter reported for the control group was 1/33.85 (1/31.69; 1/39.05), while in the experimental group it was 1/33.20 (1/33.14; 1/34.67); the value of the studied ratio for the histological specimens of the spleen in the control group was 1/24.36 (1/20.58; 1/25.61),

Table 2. White blood cell differential before implantation of the polycaprolactone diffusion chambers in the femoral neurovascular bundles of the Wistar rats and on day 40 after implantation

	Immature neutrophils	Band neutrophils	Segmented neutrophils	Eosinophils	Basophils	Monocytes	Lymphocytes
Before implantation of DC (PCL)	0%	3%	5%	0%	1%	9%	82%
	0	4%	11%	1%	0	6%	78%
	0	7%	5%	0	0	4%	84%
	0	5%	10%	0	0	8%	77%
	0	9%	14%	0	1%	8%	68%
	0	1%	14%	0	0	7%	78%
	0	3%	13%	0	1%	4%	79%
	0	1%	8%	1%	2%	6%	82%
	0	5%	18%	0	2%	6%	69%
	0	5%	12%	0	0	7%	76%
	0	5%	12%	1%	1%	6%	75%
On day 40	0	3%	5%	0	0	6%	86%
	0	1%	7%	0	2%	5%	85%
	0	8%	8%	0	0	4%	80%
	0	4%	10%	0	1%	3%	82%
	0	5%	9%	1%	1%	7%	77%
	0	4%	12%	0	0	6%	78%
	0	5%	13%	1%	0	5%	76%
	0	6%	9%	0	1%	3%	81%
	0	4%	12%	1%	0	6%	77%
	0	3%	11%	0	0	3%	83%
	0	2%	10%	0	1%	4%	83%

while in the experimental group it was 1/26.52 (1/24.39; 1/28.86); in turn, the morphometric indicator for histological specimens of the kidney was as follows: control — 1/21.87 (1/17.33; 1/28.50), experiment — 1/23.65 (1/21.78; 1/26.93).

Calculation of the white blood cell differential revealed the following characteristics: prior to implantation, lymphocyte counts were 78.00 (75.50; 80.50); monocyte counts were 6.00 (6.00; 7.50); segmented neutrophil counts were 12.00 (9.00; 13.50), which exceeded the stab form counts — 5.00 (3.00; 5.00); eosinophil counts — 0.00 (0.00; 0.50) and basophil counts — 1.00 (0.00; 1.00) were relatively low.

On day 40 after implantation the rat white blood cell differential showed a slight increase in lymphocyte counts to 81.00 (77.50; 83.00), a non-significant decrease in segmented neutrophil counts — 10.00 (8.50; 11.50), a decrease in the percentage of monocytes — 5.00 (3.50; 6.00) ($p < 0.05$).

The granulocyte and agranulocyte counts of the laboratory animals reported before and after the experiment are provided in Table 2.

DISCUSSION

Detection of macroscopic changes is possible, when the effects of the chamber and the products of its degradation are large, which indicates a rapidly developing adaptation to the foreign body [21]. The results of macroscopic assessment (appearance, slice, and capsule) of the white rat target organs, in which polycaprolactone degradation products can accumulate, reported for the experimental group have revealed no visible alterations, which suggests no effect of the PCL DC on the gross specimen structure.

The miscroscopic assessment data (structure and staining of the major histological structures, the lack of abnormal regenerative and degenerative cell forms) have not allowed us to identify alterations of the organ histoarchitectonics. Histological specimens obtained from laboratory animals of the experimental group are characterized by the typical structure without any alternative, dystrophic or necrotic changes.

The schemes of possible pathogenic changes of the studied organs (kidney, liver, spleen) resulting from the DC (PCL) implantation in the rat femoral NVB are provided in Fig. 5 [21–24], 6 [21, 25].

Thus, the alleged adrenal gland tissue pathogenesis is characterized by the septic or toxic (PCL biogedradation) damage to the tissue of the gland, abnormal increase in cortisol production, increased release of aldosterone into the bloodstream independently of the renin-angiotensin-aldosterone system, which occurs due to adrenal hyperplasia and eventually leads to hypernatremia, hypokalemia, hypertension, and metabolic acidosis [21, 26–27].

Calculation of the stromal–parenchymal relationship for the studied Wistar rat organs performed when comparing the control group and the experimental group verified no enlargement of the connective tissue component and hypo- or hyperplasia of the cellular structure of the histological specimens' parenchymal tissue. This criterion is promising for assessment of the dynamic changes in the organ morphological structure. Furthermore, its convenience lies in the universal characteristics of the tissue pool condition, which is important in cirrhotic changes of the liver, hyper- and hypofunction of both adrenal glands and the spleen, as well as for assessment of dystrophic and atrophic changes of the renal tubules and corpuscles [28].

The increase in the binucleated hepatocyte counts verifies damage to the liver parenchyma, which suggests the association of the material toxicity degree and the possibility

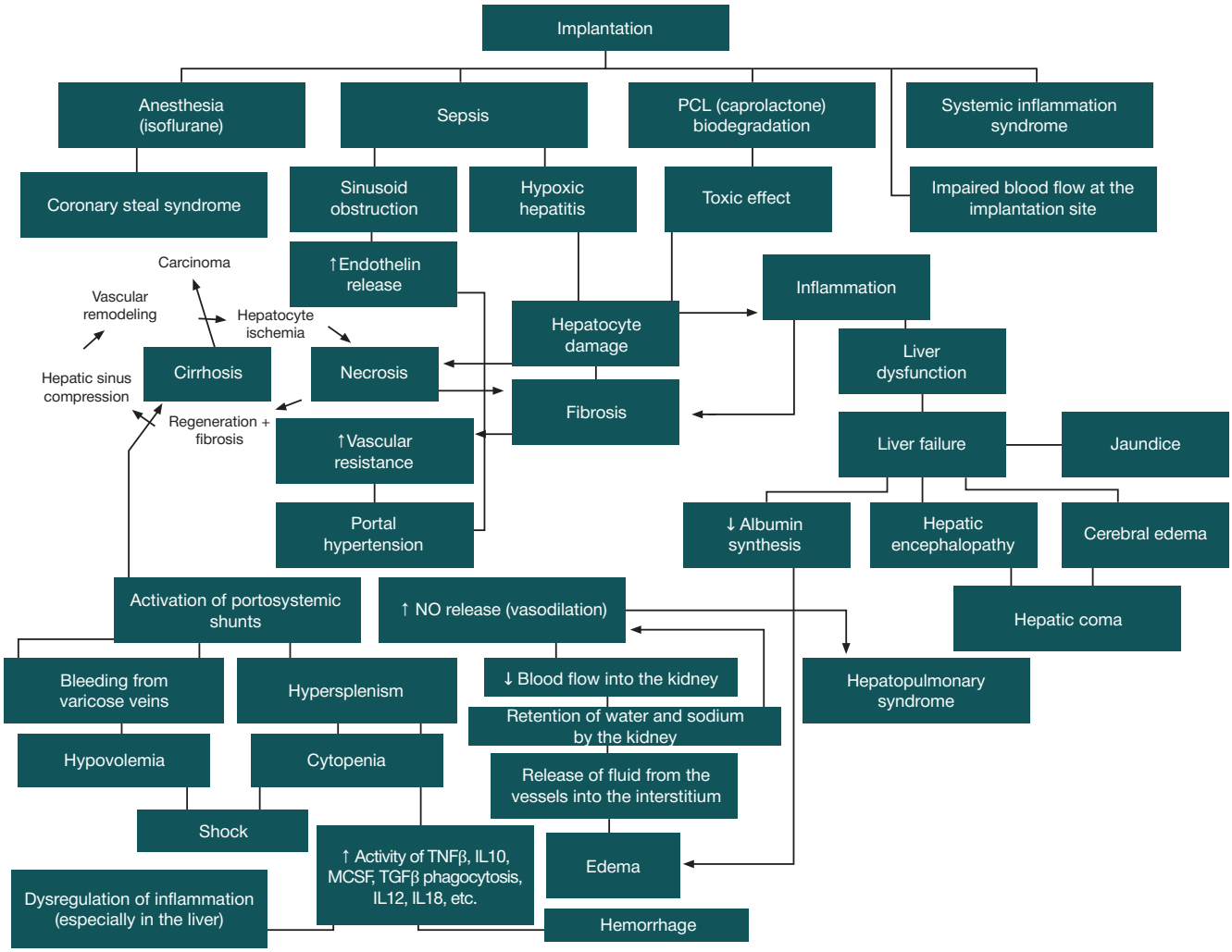

Fig. 5. Possible pathogenic changes of the liver and spleen following implantation of the PCL DC to Wistar rats [21–24]

of hepatocyte self-renewal under conditions of further longer implantation [28]. The findings also suggest that there is no active regenerative cell proliferation in the organ parenchyma.

Systemic inflammation is assessed by determining the cytokime levels [29] and peripheral blod leukogram pattern. The hemogram acquired before implantation and on day 40 after implantation is characterized by redistribution of the functionally unequal cells within the limits of physiological norm [30].

Thus, there is no chance of systemic low-grade chronic inflammation after the PCL DC implantation in the femoral NVB, which is confirmed by the use of such constructs in reconstructive surgery (arteriovenous shunts, flaps) [16], oncology (neoplastic process modeling) [19], and endocrinology (model of the pancreas).

Furthermore, it should be noted that PCL needs to be further studied at the molecular level, and the PCL study should be focused on assessing the impact of the chamber physical parameters (pore size, elasticity (including longitudinal)) on communication with the chamber microenvironment (proliferation of fibroblasts, endothelial cell growth, possible arterial hialinosis or calcification both inside the chamber and throughout the blood vessel length) and the material degradation process: rate, nature of the products obtained, main ways to neutralize and eliminate from the body. For reasons of clarity, further experiments should involve SPF animals and longer terms of implantation in order to clarify possible vascular remodeling considering the blood flow dynamics, determination of the most functional vasa vasorum, and the development of delayed post-implantation complications (thrombogenesis).

CONCLUSIONS

According to the findings, the polycaprolactone diffusion chamber installed in the femoral NVB had no adverse effect on both implantation site and the target organs. The macro- and microscopic structure of the organs of laboratory animals in the esperimental group was determined as normal structure with no alterations: no atypia, signs of inflammation or progressive degeneration of the tissues were found. Calculation of the stromal–parenchymal relationship showed that there were no abnormalities of regenerative nature: signs of fibrosis, excess angiogenesis or parenchymal expansion.

The white blood cell differential indicators determined before the experiment and on day 40 after it suggest no abnormal systemic changes in the laboratory animal body following the diffusion chamber implantation in the femoral NVB. With such a time frame, fluctuations have shown no significant differences from the pre-implantation period, which indicates sufficient isolation of the material from the body's internal environment.

The DC (PCL) used can be considered a safe engineered construct when implanted in large blood vessels,

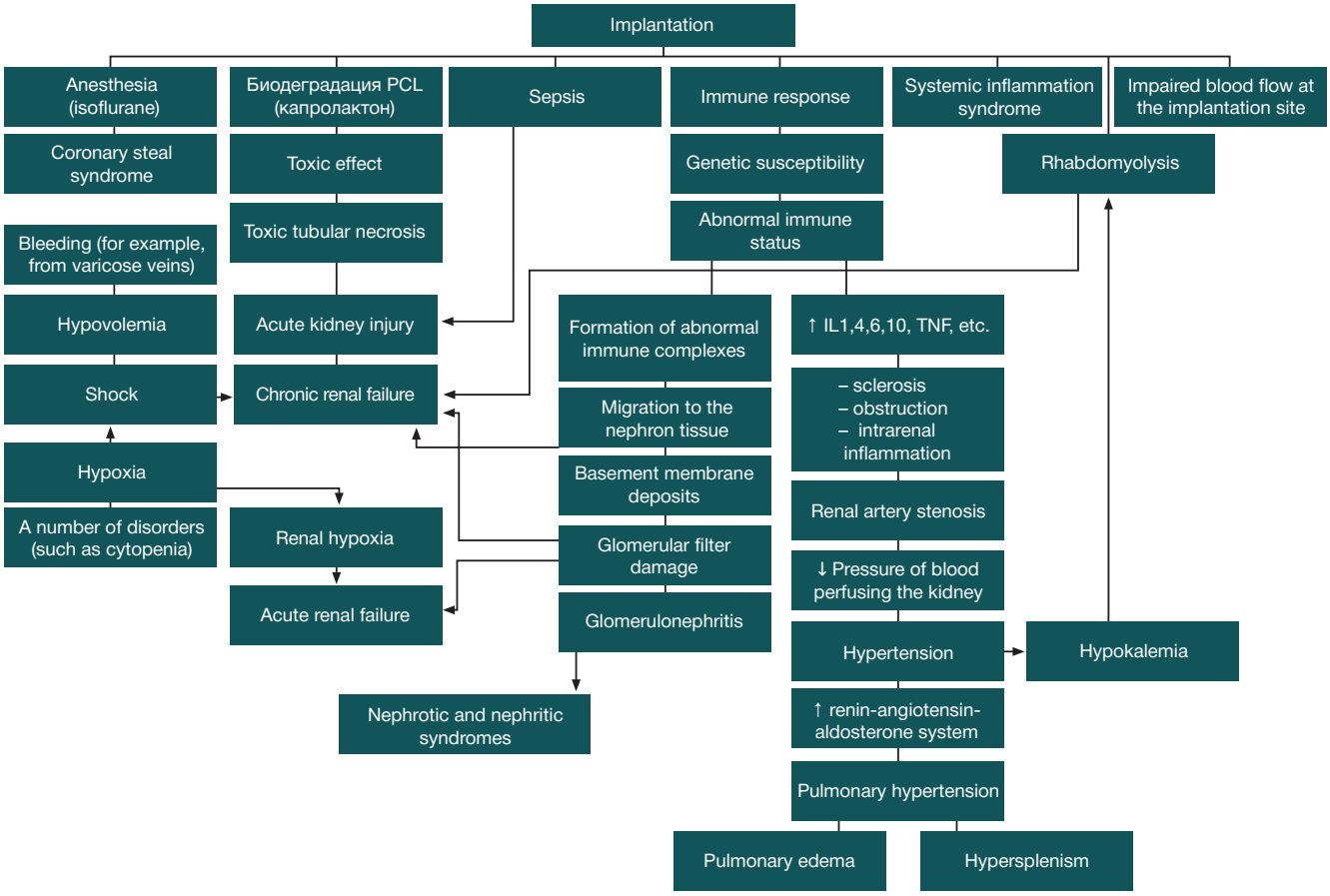

Fig. 6. Possible pathogenic changes of the kidney following implantation of the PCL DC to Wistar rats [21, 25]

specifically femoral NVB, in terms of its biocompatibility. It is important to note that assessment of the effects of the polycaprolactone biodegradation products is still relevant when choosing the research object, which requires further investigation of the PCL systemic effects during the longer biointegration period.

References

1. Abtahi S, Chen X, Shahabi S, Nasiri N. Resorbable membranes for guided bone regeneration: critical features, potentials, and limitations. ACS Mater Au. 2023; 3 (5): 394–417. PMID: 38089090; PMCID: PMC10510521.
2. Tan RP, Chan AHP, Wei S, Santos M, Lee BSL, Filipe EC, et al. Bioactive materials facilitating targeted local modulation of inflammation. JACC Basic Transl Sci. 2019; 4 (1): 56–71. PMID: 30847420; PMCID: PMC6390730.
3. Chen Tingting, Cai Tongjiang, Jin Qiao, Ji Jian. Design and fabrication of functional polycaprolactone. E-Polymers. 2015; 15 (1): 3–13.
4. Mkhabela Vuyiswa, Sinha Ray Suprakas. Poly(ε-caprolactone) nanocomposite scaffolds for tissue engineering: A brief overview. Journal of nanoscience and nanotechnology. 2014; 14 (1): 535–45.
5. Liu Fengyuan, Vyas Cian, Poologasundarampillai Gowsihan, Pape Ian, Hinduja Srichand, Mirihanage Wajira, Bartolo Paulo. Structural evolution of PCL during melt extrusion 3D printing. Macromolecular Materials and Engineering. 2017; 303 (2): 1700494.
6. Lebedeva AI, Maraeva EV. Osnovnye tendencii sozdanija kompozitnyh 3d-skaffoldov na osnove polikaprolaktona i gidroksiapatita. Nauka nastojashhego i budushhego. 2021; (1): 98–101. Russian.
7. Kazanceva EA. Konstruirovanie i ocenka jeffektivnosti sistem kontroliruemoj dostavki sel'skohozjajstvennyh preparatov razlichnogo dejstvija [dissertacija]. Krasnojarsk, 2018. Russian.
8. Homenjuk S. V. Morfologija regeneratornyh processov pri implantacii kollagenovogo materiala s adsorbirovannymi mul'tipotentnymi stromal'nymi kletkami [dissertacija]. Novosibirsk, 2023. Russian.
9. Emily Archer, Marissa Torretti, Samy Madbouly. Biodegradable polycaprolactone (PCL) based polymer and composites. Physical Sciences Reviews. 2021; (8): 4391–414. Available from: https://doi.org/10.1515/psr-2020-0074.
10. Xiang Z, Guan X, Ma Z, Shi Q, Panteleev M, Ataullakhanov FI. Bioactive engineered scaffolds based on PCL-PEG-PCL and tumor cell-derived exosomes to minimize the foreign body reaction. Biomater Biosyst. 2022; 6 (7): 100055. DOI: 10.1016/j.bbiosy.2022.100055. PMID: 36824486; PMCID: PMC9934494.
11. Luo L, He Y, Chang Q, Xie G, Zhan W, Wang X, et al. Polycaprolactone nanofibrous mesh reduces foreign body reaction and induces adipose flap expansion in tissue engineering chamber. Int J Nanomedicine. 2016; 12 (11): 6471–83. DOI: 10.2147/IJN.S114295. PMID: 27980405; PMCID: PMC5147407.
12. Fairag R, Li L, Ramirez-GarciaLuna JL, Taylor MS, Gaerke B, Weber MH, et al. A composite lactide-mineral 3D-printed scaffold for bone repair and regeneration. Front Cell Dev Biol. 2021; 7 (9): 654518. DOI: 10.3389/fcell.2021.654518. PMID: 34307346; PMCID: PMC8299729.
13. Prabhath A, Vernekar VN, Vasu V, Badon M, Avochinou JE, Asandei AD, et al. Kinetic degradation and biocompatibility evaluation of polycaprolactone-based biologics delivery matrices for regenerative engineering of the rotator cuff. J Biomed Mater Res A. 2021; 109 (11): 2137–53. DOI: 10.1002/jbm.a.37200. Epub 2021 May 11. PMID: 33974735; PMCID: PMC8440380.
14. Duda S, Dreyer L, Behrens P, Wienecke S, Chakradeo T,

Glasmacher B, et al. Outer electrospun polycaprolactone shell induces massive foreign body reaction and impairs axonal regeneration through 3D multichannel chitosan nerve guides. Biomed Res Int. 2014; 2014: 835269. DOI: 10.1155/2014/835269. Epub 2014 Apr 9. PMID: 24818158; PMCID: PMC4000981.
15. Bereshhenko VV, Nadyrov JeA, Lyzikov AN, Petrenjov DR, Kondrachuk AN. Tkanevye reakcii podkozhnoj kletchatki v otvet na implantaciju polipropilenovogo jendoproteza, modificirovannogo rastvorom polikaprolaktona metodom jelektrospinninga. Problemy zdorov'ja i jekologii. 2020; 1: 65–71. Russian.
16. Cygankov JuM, Sergeev AA, Zhorzholiani ShT, Shepelev AD, Krasheninnikov SV, Tenchurin TH, i dr. Vlijanie biomehanicheskoj sovmestimosti i trombogennosti novogo sinteticheskogo sosudistogo proteza na ego integraciju v arterial'noe ruslo (jeksperimental'noe issledovanie). Nauki o zhizni. 2021; (500): 466–9. DOI: 10.31857/S2686738921050309. Russian.
17. Mishanin AI, Panina AN, Bol'basov EN, Tverdohlebov SI, Golovkin AS. Biosovmestimost' skaffoldov iz smesej i sopolimerov polikaprolaktona i polimolochnoj kisloty v testah s mezenhimal'nymi stvolovymi kletkami. Transljacionnaja medicina. 2021; 8 (5): 38–49. DOI: 10.18705/2311-4495-2021-8-5-38-49. Russian.
18. Pankajakshan D, Krishnan VK, Krishnan LK. Vascular tissue generation in response to signaling molecules integrated with a novel poly(epsilon-caprolactone)-fibrin hybrid scaffold. J Tissue Eng Regen Med. 2007; 1 (5): 389–97. DOI: 10.1002/term.48. PMID: 18038433.
19. Ivanov AN, Chibrikova JuA, Saveleva MS, Rogozhina AS, Norkin IA. Ocenka biosovmestimosti polikaprolaktonovyh skaffoldov, obespechivajushhih adresnuju dostavku shhelochnoj fosfatazy. Citologija. 2020; 62 (12): 903–12. DOI 10.31857/S0041377120120032. Russian.
20. Bogdanov LA, Kutihin AG. Optimizacija okrashivanija jelementov sistemy krovoobrashhenija i gepatoliena l'noj sistemy gematoksilinom i jeozinom. Fundamental'naja i klinicheskaja medicina. 2019; 4 (4): 70–77. Russian.
21. Novickij VV, Urazova OI. Patofizilogija. M.: Izd-vo «GJeOTAR-Media», 2022; T. 2: 592 s. Russian.
22. Chunpeng Nie Yan Yu. Cirrhosis: pathogenesis and complications, 2022. Calgary: The Calgary guide to understanding disease; c2024 [cited 2024 March 22]. Available from: https://calgaryguide.ucalgary.ca/cirrhosis-pathogenesis-and-complications/.
23. Yunfu Lv, Wan Yee Lau, Yejuan Li, Jie Deng, Xiaoyu Han, Xiaoguang Gong, et al. Hypersplenism: History and current status. Exp Ther Med. 2016; 12 (4): 2377–82. DOI: 10.3892/etm.2016.3683.
24. Yasuko Iwakiri. Pathophysiology of portal hypertension. Clin Liver Dis. 2014; 18 (2): 281–91. DOI: 10.1016/j.cld.2013.12.001.
25. Dane Richard, Robin Bessemer. Nephritic syndrome: pathogenesis and clinical finding, 2016. Calgary: The Calgary guide to understanding disease; c2024 [cited 2024 March 22]. Available from: https://calgaryguide.ucalgary.ca/nephritic-syndrome-pathogenesis-and-clinical-findings/.
26. Kyle Moxham. Primary aldosteronism: pathogenesis and clinical findings, 2021. Calgary: The Calgary guide to understanding disease; c2024 [cited 2024 March 23]. Available from: https://calgaryguide.ucalgary.ca/primary-aldosteronism-pathogenesis-and-clinical-findings/.
27. Samin Dolatabadi, Yan Yu. Hypercortisolemia (Cushing's syndrome): clinical findings, 2021. Calgary: The Calgary guide to understanding disease; c2024 [cited 2024 March 23]. Available from: https://calgaryguide.ucalgary.ca/hypercortisolemia-cushings-syndrome-clinical-findings/.
28. Tan L, Xu X, Song J, Luo F, Qian Z. Synthesis, characterization, and acute oral toxicity evaluation of pH-sensitive hydrogel based on MPEG, poly(ε-caprolactone), and itaconic acid. Biomed Res Int. 2013; 2013: 239838. DOI: 10.1155/2013/239838. Epub 2013 Nov 30. PMID: 24364030; PMCID: PMC3864077.
29. Galashina EA, Chibrikova JuA, Ivanov AN, Gladkova EV, Norkin IA. Biohimicheskie parametry intensivnosti sistemnoj vospalitel'noj reakcii v ocenke biosovmestimosti skaffoldov na osnove polikaprolaktona i vaterita. Vestnik medicinskogo instituta «Reaviz». 2020; 2: 98–103. Russian.
30. Kosjakova GP, Muslimov AA, Lysenko AI. Vzaimodejstvie immunnoj i nervnoj sistem pri primenenii PCI-skaffoldov v cheljustno-licevoj hirurgii. Medicinskij akademicheskij zhurnal. 2019; 19 (1): 82–84. Russian.

Литература

1. Abtahi S, Chen X, Shahabi S, Nasiri N. Resorbable membranes for guided bone regeneration: critical features, potentials, and limitations. ACS Mater Au. 2023; 3 (5): 394–417. PMID: 38089090; PMCID: PMC10510521.
2. Tan RP, Chan AHP, Wei S, Santos M, Lee BSL, Filipe EC, et al. Bioactive materials facilitating targeted local modulation of inflammation. JACC Basic Transl Sci. 2019; 4 (1): 56–71. PMID: 30847420; PMCID: PMC6390730.
3. Chen Tingting, Cai Tongjiang, Jin Qiao, Ji Jian. Design and fabrication of functional polycaprolactone. E-Polymers. 2015; 15 (1): 3–13.
4. Mkhabela Vuyiswa, Sinha Ray Suprakas. Poly(ε-caprolactone) nanocomposite scaffolds for tissue engineering: A brief overview. Journal of nanoscience and nanotechnology. 2014; 14 (1): 535–45.
5. Liu Fengyuan, Vyas Cian, Poologasundarampillai Gowsihan, Pape Ian, Hinduja Srichand, Mirihanage Wajira, Bartolo Paulo. Structural evolution of PCL during melt extrusion 3D printing. Macromolecular Materials and Engineering. 2017; 303 (2): 1700494.
6. Лебедева А. И., Мараева Е. В. Основные тенденции создания композитных 3d-скаффолдов на основе поликапролактона и гидроксиапатита. Наука настоящего и будущего. 2021; (1): 98–101.
7. Казанцева Е. А. Конструирование и оценка эффективности систем контролируемой доставки сельскохозяйственных препаратов различного действия [диссертация]. Красноярск, 2018.
8. Хоменюк С. В. Морфология регенераторных процессов при имплантации коллагенового материала с адсорбированными мультипотентными стромальными клетками [диссертация]. Новосибирск, 2023.
9. Emily Archer, Marissa Torretti, Samy Madbouly. Biodegradable polycaprolactone (PCL) based polymer and composites. Physical Sciences Reviews. 2021; (8): 4391–414. Available from: https://doi.org/10.1515/psr-2020-0074.
10. Xiang Z, Guan X, Ma Z, Shi Q, Panteleev M, Ataullakhanov FI. Bioactive engineered scaffolds based on PCL-PEG-PCL and tumor cell-derived exosomes to minimize the foreign body reaction. Biomater Biosyst. 2022; 6 (7): 100055. DOI: 10.1016/j.bbiosy.2022.100055. PMID: 36824486; PMCID: PMC9934494.
11. Luo L, He Y, Chang Q, Xie G, Zhan W, Wang X, et al. Polycaprolactone nanofibrous mesh reduces foreign body reaction and induces adipose flap expansion in tissue engineering chamber. Int J Nanomedicine. 2016; 12 (11): 6471–83. DOI: 10.2147/IJN.S114295. PMID: 27980405; PMCID: PMC5147407.
12. Fairag R, Li L, Ramirez-GarciaLuna JL, Taylor MS, Gaerke B, Weber MH, et al. A composite lactide-mineral 3D-printed scaffold for bone repair and regeneration. Front Cell Dev Biol. 2021; 7 (9): 654518. DOI: 10.3389/fcell.2021.654518. PMID: 34307346; PMCID: PMC8299729.
13. Prabhath A, Vernekar VN, Vasu V, Badon M, Avochinou JE, Asandei AD, et al. Kinetic degradation and biocompatibility evaluation of polycaprolactone-based biologics delivery matrices for regenerative engineering of the rotator cuff. J Biomed Mater Res A. 2021; 109 (11): 2137–53. DOI: 10.1002/jbm.a.37200. Epub 2021 May 11. PMID: 33974735; PMCID: PMC8440380.
14. Duda S, Dreyer L, Behrens P, Wienecke S, Chakradeo T, Glasmacher B, et al. Outer electrospun polycaprolactone shell induces massive foreign body reaction and impairs axonal regeneration through 3D multichannel chitosan nerve guides. Biomed Res Int. 2014; 2014: 835269. DOI: 10.1155/2014/835269. Epub 2014 Apr 9. PMID: 24818158; PMCID: PMC4000981.
15. Берещенко В. В., Надыров Э. А., Лызиков А. Н., Петренёв Д. Р., Кондрачук А. Н. Тканевые реакции подкожной клетчатки

в ответ на имплантацию полипропиленового эндопротеза, модифицированного раствором поликапролактона методом электроспиннинга. Проблемы здоровья и экологии. 2020; 1: 65–71.
16. Цыганков Ю. М., Сергеев А. А., Жоржолиани Ш. Т., Шепелев А. Д., Крашенинников С. В., Тенчурин Т. Х. и др. Влияние биомеханической совместимости и тромбогенности нового синтетического сосудистого протеза на его интеграцию в артериальное русло (экспериментальное исследование). Науки о жизни. 2021; (500): 466–9. DOI: 10.31857/S2686738921050309.
17. Мишанин А. И., Панина А. Н., Больбасов Е. Н., Твердохлебов С. И., Головкин А. С. Биосовместимость скаффолдов из смесей и сополимеров поликапролактона и полимолочной кислоты в тестах с мезенхимальными стволовыми клетками. Трансляционная медицина. 2021; 8 (5): 38–49. DOI: 10.18705/2311-4495-2021-8-5-38-49.
18. Pankajakshan D, Krishnan VK, Krishnan LK. Vascular tissue generation in response to signaling molecules integrated with a novel poly(epsilon-caprolactone)-fibrin hybrid scaffold. J Tissue Eng Regen Med. 2007; 1 (5): 389–97. DOI: 10.1002/term.48. PMID: 18038433.
19. Иванов А. Н., Чибрикова Ю. А., Савельева М. С., Рогожина А. С., Норкин И. А. Оценка биосовместимости поликапролактоновых скаффолдов, обеспечивающих адресную доставку щелочной фосфатазы. Цитология. 2020; 62 (12): 903–12. DOI 10.31857/S0041377120120032.
20. Богданов Л. А., Кутихин А. Г. Оптимизация окрашивания элементов системы кровообращения и гепатолиенальной системы гематоксилином и эозином. Фундаментальная и клиническая медицина. 2019; 4 (4): 70–77.
21. Новицкий В. В., Уразова О. И.. Патофизилогия. М.: Изд-во «ГЭОТАР-Медиа», 2022; Т. 2: 592 с.
22. Chunpeng Nie Yan Yu. Cirrhosis: pathogenesis and complications, 2022. Calgary: The Calgary guide to understanding disease; c2024 [cited 2024 March 22]. Available from: https://calgaryguide.ucalgary.ca/cirrhosis-pathogenesis-and-complications/.
23. Yunfu Lv, Wan Yee Lau, Yejuan Li, Jie Deng, Xiaoyu Han, Xiaoguang Gong, et al. Hypersplenism: History and current status. Exp Ther Med. 2016; 12 (4): 2377–82. DOI: 10.3892/etm.2016.3683.
24. Yasuko Iwakiri. Pathophysiology of portal hypertension. Clin Liver Dis. 2014; 18 (2): 281–91. DOI: 10.1016/j.cld.2013.12.001.
25. Dane Richard, Robin Bessemer. Nephritic syndrome: pathogenesis and clinical finding, 2016. Calgary: The Calgary guide to understanding disease; c2024 [cited 2024 March 22]. Available from: https://calgaryguide.ucalgary.ca/nephritic-syndrome-pathogenesis-and-clinical-findings/.
26. Kyle Moxham. Primary aldosteronism: pathogenesis and clinical findings, 2021. Calgary: The Calgary guide to understanding disease; c2024 [cited 2024 March 23]. Available from: https://calgaryguide.ucalgary.ca/primary-aldosteronism-pathogenesis-and-clinical-findings/.
27. Samin Dolatabadi, Yan Yu. Hypercortisolemia (Cushing's syndrome): clinical findings, 2021. Calgary: The Calgary guide to understanding disease; c2024 [cited 2024 March 23]. Available from: https://calgaryguide.ucalgary.ca/hypercortisolemia-cushings-syndrome-clinical-findings/.
28. Tan L, Xu X, Song J, Luo F, Qian Z. Synthesis, characterization, and acute oral toxicity evaluation of pH-sensitive hydrogel based on MPEG, poly(ε-caprolactone), and itaconic acid. Biomed Res Int. 2013; 2013: 239838. DOI: 10.1155/2013/239838. Epub 2013 Nov 30. PMID: 24364030; PMCID: PMC3864077.
29. Галашина Е. А., Чибрикова Ю. А., Иванов А. Н., Гладкова Е. В., Норкин И. А. Биохимические параметры интенсивности системной воспалительной реакции в оценке биосовместимости скаффолдов на основе поликапролактона и ватерита. Вестник медицинского института «Реавиз». 2020; 2: 98–103.
30. Косякова Г. П., Муслимов А. А., Лысенко А. И. Взаимодействие иммунной и нервной систем при применении PCl-скаффолдов в челюстно-лицевой хирургии. Медицинский академический журнал. 2019; 19 (1): 82–84.